Applications of Nanoparticles in Mass Spectrometry for Highly Sensitive Analysis

49

Cuilan Chang, Jialing Zhang, Ze Li, Liping Li, Linnan Xu, Xianjiang Li, Baosheng Feng, Yu Bai, and Huwei Liu

Contents

Abstract

Mass spectrometry (MS) has been one of the most successful analytical techniques as it could provide highly sensitive detection and molecular structure information by recording MS or even MS^n spectra. For MS analysis, efficient ionization, interference-free detection, and development of new ionization sources are of great concern in the fields of analytical and bioanalytical chemistry. Nanoparticles (NPs), with large surface area, specific physical and chemical properties, as well as techniques of controllable synthesis and functionalization, begin to attract more and more attentions for their potential application in MS analysis. On the one hand, NPs are useful matrixes in surface-assisted laser desorption/ionization mass spectrometry (SALDI-MS), mainly benefitting from their strong light absorption in wide range. Compared with conventional organic matrixes, NPs can eliminate the "sweet spots" and provide high signals in low-mass region. Besides, after functionalized with recognition

C. Chang • J. Zhang • Z. Li • L. Li • L. Xu • X. Li • B. Feng • Y. Bai • H. Liu (✉)
Beijing National Laboratory for Molecular Sciences, Institute of Analytical Chemistry, College of Chemistry and Molecular Engineering, Peking University, Beijing, China
e-mail: hwliu@pku.edu.cn

M. Aliofkhazraei (ed.), *Handbook of Nanoparticles*,
DOI 10.1007/978-3-319-15338-4_30

ligands, NPs would gain a strong affinity to analytes, thus enriching the target compounds and improving the detection sensitivity. So far, silicon NPs, metallic NPs, metal oxide NPs, and carbon-based NPs have demonstrated their applicability in SALDI-MS, which are summarized in the following text. On the other hand, NPs can also be used for the development of new ionization sources. Nanostructure-initiator mass spectrometry (NIMS) is a novel spatially defined mass analysis technique that uses "initiator" molecules trapped in nanostructured surfaces to release and ionize samples on the surface. Owing to the advantages of high lateral resolution, high sensitivity, matrix-free, and reduced fragmentation, it is now widely used in biochemical analysis and tissue imaging. Based on the survey of literature, the authors also discussed the prospective of NPs used in MS analysis.

Keywords

Mass spectrometry • Nanomaterials • Silicon nanomaterials • Metallic nanomaterials • Metal oxide nanomaterials • Carbon-based nanomaterials • Ionization sources • Imaging analysis

List of Abbreviations

AgNPs	Silver nanoparticles
Au@AgNPs	Silver-coated gold nanoparticles
AuNPs	Gold nanoparticles
CHCA	a-cyano-4-hydroxycinnamic acid
CNT	Carbon nanotube
CVD	Chemical vapor deposition
DESI	Desorption electrospray ionization
DHB	2,5-dihydroxybenzoic acid
DIOS	Desorption/ionization on silicon
GeND	Germanium nanodots
GO	Graphene oxide
HAS	Human serum albumin
LODs	Limit of detections
MALDI	Matrix-assisted laser desorption/ionization
MPCs	Monolayer-protected gold clusters
MRI	Magnetic resonance imaging
MS	Mass spectrometry
MSI	Mass spectrometry imaging
MWCNTs	Multiwall carbon nanotubes
NIMS	Nanostructure-initiator mass spectrometry
NPs	Nanoparticles
NW	Nanowire
OCNTs	Oxidized carbon nanotubes
PANI	Polyaniline
PECVD	Plasma-enhanced chemical vapor deposition
PET	Positron emission computed tomography

SA	Sinapinic acid
SALDI	Surface-assisted laser desorption/ionization
SIMS	Secondary ion mass spectrometry

Introduction

In the past decade, mass spectrometry (MS), especially matrix-assisted laser desorption/ionization (MALDI)-MS, was increasingly used as a powerful analytical method in many fields because it allows highly sensitive detection, high-throughput analysis, and general molecular structure information provided. Since its invention in the late 1980s [1], MALDI-MS has become an important tool in life science and can be used for analysis of various samples, such as proteins, DNA/RNA, polysaccharides, synthetic polymers, and so on [2–6]. In MALDI-MS, "matrixes" are used in large excess over the analytes to minimize sample damage from laser irradiation. The matrixes co-crystallize with analytes on the sample plate and transfer proton to analytes as they are evaporated into the gas phase under laser irradiation [7]. The most popular matrixes for MALDI-MS using a N_2 laser are organic molecules, such as 2,5-dihydroxybenzoic acid (DHB), a-cyano-4-hydroxycinnamic acid (CHCA), and sinapinic acid (SA), mainly because they have strong light absorption at 337 nm and efficient proton transfer capability [8]. Although great success has been achieved for MALDI-MS, there are several problems associated with the use of organic matrixes. Firstly, the interferences of matrix in low molecule weight region (<500 Da) in MALDI-MS have significantly limited the analysis of small molecules. Secondly, the screening of the most suitable matrix and the optimization of its amounts are time-consuming, decreasing the analytical efficiency. Thirdly, the preparation of a uniform analyte–matrix surface is a rigorous challenge: the presence of "sweet spots" is common, leading to poor shot-to-shot and sample-to-sample reproducibility, which hinders the quantitative analysis in MALDI-MS.

Nanoparticles (NPs), with large surface area, specific physical and chemical properties, as well as the development of novel techniques of controllable synthesis and functionalization [9], begin to attract more and more attentions for their potential application in this field [10]. NPs are useful matrixes in one MS mode, known as surface-assisted laser desorption/ionization mass spectrometry (SALDI-MS), mainly benefitting from their strong light absorption [11]. Compared with conventional organic matrixes, NPs can overcome two major problems: the presence of "sweet spots" and the high background signals in low-mass region. Besides, after functionalized with recognition ligands, NPs would gain a strong affinity for analytes, thus enriching the target compounds and improving the detection sensitivity. So far, silicon NPs, metallic NPs, metal oxide NPs, and carbon-based NPs have demonstrated their applicability in SALDI-MS. Additionally, NPs can also be used for the development of new ionization sources. Nanostructure-initiator mass spectrometry (NIMS) is a novel spatially defined mass analysis technique that uses "initiator" molecules trapped in nanostructured surfaces to release and ionize

samples on the surface. Owing to the advantages of high lateral resolution, high sensitivity, matrix-free, and reduced fragmentation, it is now widely used in biochemical analysis and tissue imaging.

In this chapter, the authors focus on the applications of NPs in MS for highly sensitive analysis, with the emphasis on the applications of various NPs in SALDI-MS, including silicon nanomaterials, metallic nanomaterials, metal oxide nanomaterials, and carbon-based nanomaterials. The development of NP-based new ionization sources, NIMS, was also discussed (summarized in Table 1).

Matrix Effects of NPs in SALDI-MS

With the development of nanoscience and nanotechnology, NPs of various size, shapes, and compositions (such as silicon NPs, metallic NPs, metal oxide NPs, and carbon-based NPs) have been widely used as matrixes in SALDI-MS to improve the applicability of MALDI-MS (Schematic 1).

Tanaka et al. [12] reported ultrafine 30 nm diameter cobalt powder suspension as the inorganic matrix for the MS detection of proteins for the first time. This work demonstrated that the NPs can obviously improve the sensitivity since they can capture analytes, absorb and transfer laser energy for effective desorption and ionization. On the other hand, NPs provide some MS background due to the formation of metal clusters. Although there still are some debates on the mechanisms, the most commonly accepted one is based on the thermally driven energy transfer from NPs to analytes [13]. The temperature change on NP surfaces depends on the incident laser frequency, the absorptivity of the NPs, and the diffusion of the heat during the laser pulse duration [11, 13]. A higher temperature could be generated on the surfaces of NPs with a low heat capacity upon laser irradiation. As a result, NPs with high absorptivity at the emission wavelength of the laser irradiation source, low heat capacity, and few cluster ions (low MS background) are promising in improving sensitivity of SALDI-MS. For example, when N_2 lasers are used, NPs that have substantial absorptivity near 337 nm are good candidates – such as TiO_2, Au, and Ag NPs. Also, when NPs are used to selectively capture analytes, Au and Ag NPs could form specific Au–S and Ag–S bond with thiol-containing analytes.

In the following text, the applications of various NPs in SALDI-MS for high sensitive detection are described, including silicon NPs, metallic NPs, metal oxide NPs, and carbon-based NPs.

Silicon NPs

Porous silicon was firstly reported to be capable of trapping analytes and transferring laser energy to the analytes, which were then desorbed/ionized by MS [14]. This method was termed as desorption/ionization on silicon mass spectrometry (DIOS-MS), and it was notable mainly for the use of monolithic target. In this

Table 1 Some representative examples of the use of nanomaterials in mass spectrometry for highly sensitive analysis

Nanomaterial	Functionalization	Morphology	Application	Analytes	Instruments	References
Silica NPs	Galvanostatic etching procedure	Porous silicon	On-plate detection	Peptides, antiviral drugs, etc.	MALDI-MS	[14]
	Double electrochemical etching	Porous silicon	On-plate detection	Steroid sulfates	MALDI-MS	[17]
	Plasma-enhanced chemical vapor deposition	Column/void network silicon film	On-plate detection	Peptides, ubiquitin, etc.	MALDI-MS	[20]
	Self-assembled germanium nanodots deposited on a silicon wafer	Silicon wafer	On-plate detection	Angiotensin-I, insulin, myoglobin, etc.	MALDI-MS	[21]
	Reactive ion etching	Silicon nanocavity arrays	On-plate detection	Angiotensin-I, bradykinin, Ala-Leu-Ala-Leu, Val-Met	MALDI-MS	[22]
	Chemical vapor deposition	Silicon nanowires	On-plate detection	Perfluorodecyl trichlorosilane	MALDI-MS	[23–35]
	H_2O_2 metal–HF etching	Porous silicon	On-plate detection	BSA, lyophilized desArg9-bradykinin, etc.	MALDI-MS	[26–29]
	Iodine-assisted etching	Nanostructured silicon	On-plate detection	Labetalol hydrochloride, procainamide ethylenediamine, nadolol, etc.	MALDI-MS	[32]

(*continued*)

Table 1 (continued)

Nanomaterial	Functionalization	Morphology	Application	Analytes	Instruments	References
Metal-based nanomaterials	Size-selected AuNPs	Diameter: 2, 5, 10 nm	Mix with analyte solution as matrix	Peptides and small proteins	MALDI	[44]
	Gold nanospheres, nanorods, and nanostars	Spheres, 20 nm; rods, diameter 18 nm, length 50 nm; stars, 35 nm (core), 50 nm (whole particle)	Mix with analyte solution as matrix	PEG 600	MALDI	[45]
	Gold film	10 nm thick	On-plate detection	Peptides, nucleosides, and nucleotides	MALDI	[46]
	Gold film coated on nanoporous aluminum oxide layers	Al film: 300, 400, 500, 600, 700, 900, 1,100, and 1,450 nm Gold film: 30, 90, 120, and 220 nm	On-plate detection	Peptides	MALDI	[47]
	Monolayer-protected gold nanoclusters	Core diameter: 2 nm	Mix with analyte solution as extraction and detection	Peptides	MALDI	[48]
	Boronic acid-modified gold nanoparticles	Diameter: 50–100 nm	On-plate extraction and detection	Horseradish peroxidase	MALDI	[49]
	Au@magnetic particles	AuNPs: ~16 nm	Mix with analyte solution as extraction and detection	Proteins, peptides, cationic surfactants, and tryptic digest products	MALDI	[50]

	AgNPs	34 ± 3 nm	Mix with analyte solution as extraction and detection	Three estrogens	MALDI	[51]
	Au@AgNPs	39 ± 5 nm	Mix with analyte solution as extraction and detection	Aminoglycosides	MALDI	[52]
	Pt nanoflower	Single nanometer level	Mix with analyte solution as matrix	Peptides and phospholipids	MALDI	[53]
	Pt Nfs on scratched silicon substrate	Pt Nfs: 100–300 nm	Mix with analyte solution as matrix	Phospholipids, synthetic polymers, peptides, and so on	MALDI	[55]
Metal oxide NPs	Homogeneous TiO_2 layer	50 nm thick	On-plate detection	Sugars and metabolic analysis	MALDI-MS	[56]
	TiO_2 nanotube layers	0.5, 1.0, or 2.0 μm long	On-plate detection	Peptides	MALDI-MS	[57]
	Fe_3O_4@TiO_2 NPs	50 nm	Mix with analyte solution as matrix	Phosphopeptides	MALDI-MS	[58]
	TiO_2 NPs	5 ± 1 nm	Mix with analyte solution as matrix	Enediol compounds	MALDI-MS	[59]
	Catechin-modified TiO2 NPs	Less than 20 nm	Mix with analyte solution as matrix	Steroid hormones	MALDI-MS	[60]
	TEOS–TiO_2	Less than 50 nm	Mix with analyte solution as matrix	Photocatalytic degradation of PEG	MALDI-MS	[61]
	TiO2 NPs	Less than 10 nm (estimated)	Deposited on tissue surface	Mouse brain tissue	MALDI-MS	[62]
	ZnO NOs	Anisotropic shapes	Mix with analyte solution as matrix	Various small molecules	MALDI-MS	[63]

(*continued*)

Table 1 (continued)

Nanomaterial	Functionalization	Morphology	Application	Analytes	Instruments	References
	ZnO nanowires	25–1,600 nm long	On-plate detection	Various small molecules	MALDI-MS	[64]
	Silanized Fe_3O_4 NPs	10–20 nm (estimated)	Mix with analyte solution as matrix	Peptides	MALDI-MS	[65]
	HSA-modified Fe_3O_4 NPs	20–50 nm	Mix with analyte solution as matrix	Drugs	MALDI-MS	[66]
	TiO_2–WO_3	Mesoporous, average pore size 9.8 nm	On-plate detection	Gramicidin S	MALDI-MS	[67]
	TiO_2, TiSiO, BaSrTiO NPs	Commercial	Mix with analyte solution as matrix	Neutral carbohydrates	MALDI-MS	[68]
Carbon NPs	Pristine CNTs	Rod, outer diameter of ~20 nm and inner diameter of ~2 nm	Mix with analyte solution as matrix	Peptides, organic compounds, and β-cyclodextrin	MALDI-MS	[73]
	Pristine CNTs	Diameters of ca. 250 nm and tube lengths of ca. 60 μm	Mix with analyte solution as matrix	Small proteins and peptides	MALDI-MS	[74]
	OCNTs	–	Mix with analyte solution as matrix	Oligosaccharides, peptides, and insulin	MALDI-MS	[75]
	OCNTs	–	Mix with analyte solution as matrix	Jatrorrhizine and palmatine	MALDI-MS	[76]
	MWCNTs@PANI	Rough surface covered by PANI pellets with a thickness of about 5 nm	Mix with analyte solution as matrix	Small metabolites	MALDI-MS	[77]

	2,5-Dihydroxybenzoyl hydrazine-derived CNTs	Less twist in basic condition than in neutral condition	Mix with analyte solution as SPE sorbent and SALDI matrix	Peptides	MALDI-MS	[78]
	MWCNT/CdS NPs	Rodlike, composited with several cylindrical graphite sheets and the CdS NPs in neutral condition	Mix with analyte solution as SPE sorbent, SALDI matrix, and heat-adsorbing material for microwave-assisted digestion	Peptides and proteins	MALDI-MS	[79]
	Fe_3O_4@SiO_2/OCNTs	–	Mix with analyte solution as SPE sorbent and mix with analyte solution as matrix	Benzo[α]pyrene	MALDI-MS	[80]
	C_{60}	–	Mix with analyte solution as matrix	Uranium	MALDI-MS	[83]
	C_{60} and C_{70}	–	Mix with analyte solution as matrix	Nonderivatized steroids	MALDI-MS	[84]
	Hexa(sulfonbutyl)fullerene, $C_{60}[(CH_2)_4SO^{3-}]_6$	–	Mix with analyte solution as precipitating reagent and SALDI matrix	Positively charged surfactants, amino acids, peptides, and proteins	MALDI-MS	[85]
	Acidic functionalized fullerene, $C_{60}[(CH_2)_2COOH]_n$	–	Mix with analyte solution as matrix	Peptides	MALDI-IM-oTOF-MS	[86]

(*continued*)

Table 1 (continued)

Nanomaterial	Functionalization	Morphology	Application	Analytes	Instruments	References
	Dioctadecyl methano[60] fullerene, [60]fullerenoacetic acid, and IDA-[60]-fullerene	–	Mix with analyte solution as matrix and SALDI matrix	Low-mass serum constitute	μ-HPLC, MALDI-MS, and ESI-MS	[87]
	Graphene	Flake	Mix with analyte solution as matrix	Amino acids, polyamines, etc.	MALDI-TOF MS	[92]
	Graphene	Flake	Mix with analyte solution as matrix	Amino peptides, acids, and fatty acids	MALDI-TOF MS	[93]
	Graphene and GO	Flake	Mix with analyte solution as matrix	ssDNA	SELDI-TOF MS	[94]
	Graphene	Flake	Mix with analyte solution as matrix	Polycyclic aromatic hydrocarbons and estrogen	MALDI-TOF MS	[95]
	Graphene, GO, and reduced GO	Flake	On-plate detection	Flavonoids and coumarin	SELDI-TOF MS	[96]
	Reduced GO coated on SiO_2 substrate	Film	On-plate detection	Octachlorodibenzo-*p*-dioxin	MALDI-TOF MS	[97]
	Graphene and GO	NM	Mix with analyte solution as matrix	Tetracycline	MALDI-TOF MS	[98]
	Aptamer-conjugated GO	Solution	Mix with analyte solution as matrix	Cocaine and adenosine	MALDI-TOF MS	[99]
	GO/CNT coated on substrate	Double layer	Mix with analyte solution as matrix	Phospholipids	LDI-TOF MS	[100]
	Magnetic graphene composites	Flake	Mix with analyte solution as matrix	Luteoloside and nicotine nitrogen oxides	MALDI-TOF MS	[101]
	Magnetic graphene and CNT	Flake and multiwall	Mix with analyte solution as matrix	Sucrose, amino acid, etc.	MALDI-TOF MS	[102]

Nanostructure-initiator mass spectrometry (NIMS)	P-type ⟨100⟩ (boron) silicon with initiator BisF17	10 nm pores	Laser-NIMS	Single cancer cell, tissues, and biofluids	MALDI	[110]
	P-type ⟨100⟩ (boron) silicon silanized with a 14-kDa poly (3,3,3-trifluoropropylmethylsiloxanes) polymer	10 nm pores	Ion-NIMS	Peptide	TOF-SIMS	[110]
	P-type ⟨100⟩ (boron) silicon with initiator BisF17	10 nm pores	Laser-NIMS	Clozapine, *N*-desmethylclozapine, ketamine, and norketamine	MALDI	[111]

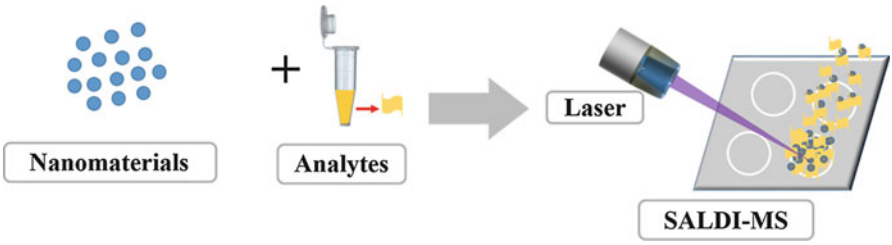

Schematic 1 Applications of nanoparticles in SALDI-MS

work, porous silicon was acquired through a galvanostatic etching procedure, and the results showed that DIOS-MS can provide higher sensitivity and less or no fragmentation. Different chemical and structural modifications of the silicon surface were studied, indicating that the surfaces with smaller pore sizes and more hydrophobicity gave better signals.

DIOS-MS has opened a new chapter for the development of SALDI-MS [15, 16]. Since then, several groups investigated the preparation conditions of porous silicon [17–19]. Electrochemical etching is the most commonly used method in literatures. For instance, Shen et al. [17] found that double etching could enhance the sensitivity, but the analytes needed to be desorbed with higher laser energy; wet chemical etching approaches could produce substrates exhibiting substantial inter-sample variability. Later, plasma-enhanced chemical vapor deposition (PECVD) was used to form column/void network silicon film [20]. The appropriate thickness of the film should be between 50 and 100 nm to obtain efficient desorption/ionization of the analytes. Through molecular beam epitaxy, self-assembled germanium nanodots (GeND) could be deposited on a silicon wafer [21]. The upper limit of detectable mass range was ~17 kDa using GeND-MS. Reactive ion etching was also utilized to generate ordered silicon nanocavity arrays [22], and it was capable of systematically varying surface geometries to acquire desired features. Other techniques, such as chemical vapor deposition (CVD) [23–25], H_2O_2 metal–HF etching [26–29], silver-assisted chemical etching [30, 31], and iodine-assisted etching [32], have also been explored.

In recent years, some improvements to DIOS-MS were made. For example, silver (Ag) NP-coated porous silicon presented much higher stability, sensitivity, and reproducibility than untreated porous silicon [33]. Mathieu Dupré et al. [34] studied the influences of silicon surfaces with different morphologies and chemical functionalizations on the performance of laser desorption/ionization in detail, demonstrating that surface with two nanostructured layers provided the best performance. Besides, there are also a few reports on SALDI-MS occurring on flat surfaces, such as flat surface of amorphous silicon [35] and commercial silicon-on-insulator wafers [36].

In addition to the methods mentioned above, there are still a few techniques employing silica as matrix. Silica gel bounding with DHB and HCCA was able to improve the intensity of MS [37]. More recently, a cost-efficient method

acquired femtomole sensitivity by depositing silica nanoparticles on conventional MALDI target plate [38]. Other works utilizing bare silica nanoparticles [39], C-18-functionalized magnetic silica nanoparticles [40], amorphous silica nanoparticles [41], zirconium arsenate-modified silica nanoparticles [42], and magnetic core–shell silica nanoparticles [43] were also reported.

To sum up, various forms of silicon or silica have been utilized in MS to enhance the sensitivity. Considering silicon is a cost-efficient material, it is fully believed that silicon or silica-related MS techniques must have a bright future.

Metallic NPs

In this section, the authors will summarize the applications of precious metals in SALDI-MS. Among them, Au nanomaterials with good biocompatibility could form Au–S covalent bonds with thiol groups on biomolecules. They have been widely used as matrix for signal enhancement in SALDI-MS, and they were also used as enrichment probe for target molecules.

Various nanostructures, such as Au nanorods [44], Au nanospheres [45], Au nanostars [45], Au films [46], composite Au materials, etc., could be obtained with controllable synthesis. Many researchers studied the relationship between nanostructure morphologies (particles and films) and the maximum absorbance wavelengths. Mclean et al. investigated size-selected AuNPs and found that the relative abundances of the ions in positive and negative mode showed significant differences as the AuNP size distribution decreased from 10 to 2 nm [45]. When gold films were used as matrix, the film thickness was tuned in order to match its maximum absorbance to the excitation laser wavelength [46]. For Au film-coated nanoporous alumina composite substrates, several factors including Au layer thickness, alumina pore size, and geometry all had effects on the energy absorption and transfer efficiency [47]. Six hundred and ninety nanometers were found to be the optimum thickness for alumina substrates and gold layer, respectively.

Gold NPs have also been used as sorbents and matrix in SALDI-MS simultaneously. Gold surface was easy to form gold–sulfur bonds and generate self-assembled monolayer-protected Au nanomaterials, which were named monolayer-protected gold clusters (MPCs). MCPs provide many desirable attributes for selective extraction. Benjamin et al. [48] prepared cationic and anionic ligand-decorated MPC(+) and MPC(−) for selectively extracting peptides at varying pI through electrostatic interactions, and this method can detect peptides as low as 500 pM in 250 μL solutions. Moreover, on plate strategies have also been proposed. In Zhang's group [49], gold NPs were first spotted and sintered on a stainless steel plate and then modified with 4-mercaptophenylboronic acid to selectively enrich glycopeptides containing *cis*-1,2-diol groups. After enrichment and washing off nonspecific peptides, target analytes were directly determined. Due to the existence of AuNPs, the laser absorbance efficiency was more effective, resulting in higher desorption and ionization efficiency. Magnetic separation has also been introduced into this field. In 2004, Teng et al. [50] first described a

strategy using Au@Fe_3O_4 nanoparticles with negative-charged surfaces to capture positive-charged proteins from aqueous solutions. Compared with traditional centrifugation, Au@Fe_3O_4 could be easily separated from solution by applying an external magnet. After washing, analytes can be directly analyzed without elution by SALDI-MS with AuNPs as matrix.

Besides, other precious metals were also reported in SALDI-MS. AgNPs have extremely high absorption coefficients at 337 nm, which is near the maximum wavelength of the nitrogen laser. Chiu et al. [51] applied AgNPs as matrixes for the determination of three small molecules – estrone, estradiol, and estriol. The limit of detections (LODs) can be as low as 0.23 μM for estradiol, and the shot-to-shot and batch-to-batch variations for the three analytes were less than 9 % and 13 %. Also, silver-coated AuNPs (Au@AgNPs) were used to extract analytes in plasma samples by electrostatic attractions, which provide low LOD and high recoveries [52].

Arakawa et al. [53] synthesized surface clean platinum nanomaterials with thin projections on the PtNPs surface, termed Pt nanoflowers. Using this new material, one can obtain higher sensitivity for peptides and phospholipids with lower laser energy and smaller sample amounts (a few femtomoles). The matrix effects of different bare metals (Cu, Ag, Au, and Pt) prepared by laser ablation were systematically investigated. For desorption/ionization of a representative peptide, angiotensin 1, PtNPs exhibited the best performance in SALDI-MS owing to their smaller heat conductivity and higher melting temperature [54]. What is more, Pt composite materials were also investigated. The surface modified Pt Nf silicon hybrid plate was found to facilitate detections of labile compounds. This plate has been proved to be a high-affinity substrate for phosphopeptides. Excellent detections were achieved for β-casein digest and various analytes [55].

Metal Oxide NPs

There are certain kinds of metal oxides, such as TiO_2, Fe_3O_4, and ZnO, reported as matrixes of SALDI-MS. TiO_2 is considered as one of the most promising materials in SALDI-MS because of its strong absorption in UV region. Recently, Sonderegger et al. [56] coated a stainless steel target with a 50 nm homogeneous TiO_2 layer and investigated its ability to desorb small molecules. For the analysis of sugars, the peaks were mainly cationized by sodium and potassium instead of protonated. In addition, this TiO_2-coated target can be used repeatedly as an ideal choice for metabolic analysis. Piret et al. [57] applied TiO_2 nanotube layers with different lengths (0.5, 1.0 and 2.0 μm) prepared by electrochemical anodization of Ti foil, finding that the shortest nanotube layer (0.5 μm) showed the best performance in SALDI-MS analysis.

Besides SALDI-MS effect, TiO_2 nanomaterials were also frequently reported as concentration probes for some specific analytes, making it possible to work in both analyte enrichment and signal enhancement. For example, Fe_3O_4@TiO_2 core–shell NPs were used to extract phosphopeptides from protein digests, and after magnetic separation, the Fe_3O_4@TiO_2 NPs acted as the matrix in MALDI-MS analysis [58].

Benefitting from the enrichment process and the signal enhancement effect, the LOD was in the femtomole range, and the upper detectable mass limit was ~24,000 Da. Similarly, TiO_2 was also used to selectively enrich, desorb, and ionize catechins [59]. The interactions between enediol compounds and TiO_2 NPs were evident from the color change from milky white to orange, which also resulted in the increase of UV absorbance. Therefore, the energy transfer in SALDI-MS process turned to be more effective. Furthermore, the interactions between TiO_2 and catechins can be utilized to obtain catechin-modified TiO_2, and the absorption at 337 nm laser was further increased. Researchers proved that this material showed excellent effect in the analysis of four steroid hormones [60], including cortisone, hydrocortisone, progesterone, and testosterone. The quantitative data showed good sensitivity and reproducibility, indicating the practicality and simplicity of this approach.

In particular, the applications of TiO_2 in SALDI-MS have been extended recently. In 2009, the additives in a mixtures produced by photocatalytic degradation of PEG were directly analyzed by TiO_2-based SALDI-MS [61]. Later, successful imaging of endogenous low molecular weight metabolites (80–500 Da) in mouse brain using TiO_2 NPs was reported [62]. During the detection and imaging process, there was no need for any wash or separation steps, which made the method simple, practical, and more powerful than those using DHB or AuNPs as matrix.

ZnO was also proved to have SALDI effect, and further developments are still in process. Ryuichi Arakawa et al. [63] developed a SALDI method using ZnO NPs with anisotropic shapes, and various small molecules, including verapamil hydrochloride, testosterone, and polypropylene glycol (average molecular weight 400), were successfully detected without using a liquid matrix or buffers. The author pointed out that the ZnO-based SALDI-MS has advantages in post-source decay analysis and produced a simple mass spectrum for phospholipids. Recently, Shin et al. [64] investigated the effects of nanowire (NW) length on SALDI-MS analysis of small molecules. In their work, ZnO NWs of different lengths ranging from 25 to 1,600 nm were fabricated on an Au-/Ti-/Si-structured substrate by a vapor transport process, and the results suggested that the nanostructure was essential for SALDI process. The authors discussed the influences of NW length mainly from the aspect of effective energy transfer, and their conclusion may offer valuable insight for searching and tailoring novel nanostructures for SALDI materials.

For Fe_3O_4-based SALDI-MS applications, Chen et al. [65] used silane-immobilized magnetic iron oxide particles to analyze small proteins and peptides, showing that the LOD of peptides was as low as ~20 fmol and the upper mass limit was 16,000 Da. Furthermore, after functionalized with negative charge ligands, the Fe_3O_4 NPs can act as affinity probes to selectively trap positive-charged compounds in complex solutions by the electrostatic interactions. Iwaki et al. [66] modified the Fe_3O_4 nanoparticles with human serum albumin (HSA), and the obtained material was an effective affinity-based SALDI matrix for the analysis of drugs in human biological liquids. The successful capture of several small drugs (phenytoin, ibuprofen, camptothecin, and warfarin sodium) via HSA–drug interactions was demonstrated. Benefitting from the SALDI effect of Fe_3O_4, the detection

sensitivity for the four drugs was higher than that with an organic matrix. This affinity-based SALDI-MS using protein-modified Fe_3O_4 NPs offers new approaches for the drug analysis in biological liquids.

Besides the commonly used TiO_2, ZnO, and Fe_3O_4, the use of other metal oxides was also under investigation at the same time, and most of them were the extension of TiO_2-based SALDI-MS methods. For example, mesoporous TiO_2–WO_3 was synthesized by an "acid–base pair" strategy using $EO_{106}PO_{70}EO_{106}$ as a structure-directing agent. This material had high porosity with a pore size of 9.8 nm and a large BET surface of 150 m^2/g, and the spectrum exhibited an intense absorbance at 340 nm. The results showed that the signal intensities using mesoporous TiO_2–WO_3 were about hundred folds than those using nonporous WO_3–TiO_2 as the matrix [67]. In another report, diamond, TiO_2, TiSiO, BaSrTiO NPs, and their mixtures were applied as the matrix for profiling of neutral carbohydrates in tissues [68], and the LODs were sufficient for the analysis of soluble carbohydrates in fresh plant. In this work, researchers also pointed out that the varied performances of laser desorption/ionization capability were mainly resulted from their different sizes, compositions, structures, and chemical/photochemical properties.

In summary, various metal oxide nanomaterials, such as NPs, nanotubes, or those with porous structures, have been applied in SALDI-MS. Among these reports, some metal oxides can be further used as affinity probes directly or after proper modification. Considering the large metal oxide family with diverse functionalization forms, the authors believe that the potential of metal oxide-based SALDI is far from fully discovered.

Carbon NPs

Carbon nanotube (CNT) with a tubelike cylindrical nanostructure is promising in many application fields because of their extraordinary electrical, optical, mechanical properties and thermal conductivity [69–72]. Its conjugated carbon wall facilitates the energy absorption and transfer, making CNT an ideal matrix in SALDI-MS. In 2003, Xu et al. [73] first used CNTs prepared from coal by arc discharge to trap peptides, organic compounds, and β-cyclodextrin and then as matrix for the analysis of these analytes. The use of CNTs as matrix eliminated the interference of matrix signal and reduced fragmentation remarkably. Chen et al. [74] employed CNTs produced from a reactive anodic aluminum oxide template as SALDI-MS matrix for the analysis of some small proteins and peptides, showing that the addition of high-concentration citrate buffer not only reduced the alkali adduct ions but also extended the mass range.

Pristine carbon nanotubes have poor solubility in water. When they are used as matrix directly, it is hard to form homogeneous layers with analytes on the target, resulting in poor reproducibility of data. To solve this problem, oxidized carbon nanotubes (OCNTs), as the oxidation form of CNTs, are employed. The increased polarity and solubility of OCNTs help the dispersion of matrix in water, thus

enhancing the reproducibility. In addition, the carboxyl groups on the surface of OCNTs can also act as proton sources, improving the ionization efficiency of analytes. Ren et al. [75] synthesized OCNTs by treating CNTs with nitric acid, and the OCNTs were used as matrix for the SALDI-MS analysis of oligosaccharides, peptides, and insulin. Pan et al. [76] prepared OCNTs by oxidization of CNTs with HNO_3/H_2SO_4 mixture, which were then used for the analysis of jatrorrhizine and palmatine. Other surface modifications of CNTs can also help in improving the dispersity. Meng et al. [77] proposed a novel hydrothermal synthesis for preparation of the composites of multiwall carbon nanotubes (MWCNTs) and polyaniline (MWCNTs@PANI). MWCNTs were firstly treated with nitric acid to create carboxylic groups on the outer surface, and aniline was polymerized and covalently bonded with the MWCNTs via a hydrothermal reaction. The MWCNTs@PANI with higher dispersity in water was used as matrix for the detection of six small metabolites, resulting in high sensitivity and reproducibility.

Besides improving the dispersity, modification of surface of CNTs can also contribute to the adsorption property and SALDI-MS analysis of special molecules. Ren et al. [78] derivatized CNTs with 2,5-dihydroxybenzoyl hydrazine. The functionalized CNTs were used as a pH adjustable enriching reagent and matrix for SALDI analysis of trace peptides. Shrivas et al. [79] modified MWCNTs with hydrosulphonyl groups and then added $Cd(NO_3)_2$ and Na_2S solution in sequence to get a MWCNTs/CdS NPs. When solution pH is higher than the pI of the peptides and proteins, electrostatic interaction between negatively charged peptides/proteins and positively charged NPs occurs. This MWCNTs/CdS can be used as preconcentrating probes, MALDI matrix, and heat-adsorbing material for the analysis of microwave tryptic digestion of proteins.

When CNTs were used as extraction reagent before as matrix for MALDI analysis, the separation of CNTs from solution is of high values. Li et al. [80] synthesized a magnetite/OCNTs composite, $Fe_3O_4@SiO_2$/OCNTs, by simply mixing $Fe_3O_4@SiO_2$ and OCNT in *N*,*N*-dimethylformamide, to facilitate the separation after extraction. The composite was used as a solid-phase extraction adsorbent and then as a MALDI matrix for the analysis of benzo[α]pyrene, which was hardly ionized by MALDI and ESI.

Fullerene, often refers to spherical fullerene, is also an important class of carbon material with unique ball structure and superconductivity [81, 82]. Owing to its conjugated carbon surface and UV absorption activity, fullerene can also be used as extraction adsorbent and matrix for SALDI-MS. Havel et al. [83] used C_{60} cluster as SALDI matrix for the determination of uranium. The sensitivity of uranium determination via UO_2^{2+} was increased by the usage of C_{60} as matrix with the LOD of 5×10^{-8} mol L^{-1}. Montsko et al. [84] used C_{60} and C_{70} as matrix for SALDI-MS analysis of nonderivatized steroids. More effective ionization and higher signal intensity were obtained when fullerene, especially C_{70}, rather than traditional organic acid, was used as matrix.

Derivation of fullerene can also expand its applications for multiple substances analysis. Shiea et al. [85] synthesized a water-soluble fullerene derivative by treating C_{60} with sodium naphthalide followed by treating the resulted anionic

fullerene intermediates with an excess of 1,4-butane sultone. The fullerene derivative has six negatively charged sulfonate arms, which can precipitate positively charged surfactants, amino acids, peptides, and proteins by electrostatic interaction. Then, the precipitate can be directly analyzed by SALDI-MS with the derivatized fullerene as matrix. Ugarov et al. [86] suspended an acidic functionalized fullerene in water/ethanol solution by sonication, which was derivatized with carboxyl groups by the peroxide oxidation. The functionalized fullerene was then used as matrix solution for peptides analysis by SALDI-MS. Vallant et al. [87] synthesized fullerene derivatives, including dioctadecyl methano[60]fullerene, [60] fullerenoacetic acid, and IDA-[60]-fullerene, for the enrichment and analysis of low-mass serum constitute. These derivative fullerenes could interact with the combination of serum constitute by reversed phase, ion exchange, and immobilized metal ion affinity adsorption mechanism, respectively.

Graphene and graphene oxide (GO) are twin brothers; in other words, they can convert to each other in different conditions. Oxidant can change graphene to GO and vice versa. The concept of graphene can date back to 1986 by Boehm [88]. After 18 years of breeding, it was finally born in 2004 by mechanical exfoliation [89]. Since then, many scientists devoted to this new star, and great achievements were accomplished in short time. That is because this strictly two-dimensional material has its excellent properties, such as strong ambipolar electric field, high carrier mobilities, exceptional Young modulus values, large spring constants, high specific surface, and so on [89].

Graphene and GO could be prepared by physical or chemical methods [90]. Physical methods mainly include micromechanically cleavage, liquid exfoliation, and SiC sublimation. Chemical method mainly contains chemical vapor deposition, epitaxial growth, organic synthesis, and reduction of GO. Probably, the most common used and inexpensive way is the reduction of GO, a modified Hummer method [91].

Graphene's large surface area helps to trap analytes, and its conjugated structure is effective in absorbing and transferring energy to the analytes upon laser irradiation, which allows the analytes to be readily desorbed/ionized. It can significantly increase the signal intensity and reduce the fragmentation of the analytes. Dong et al. [92] used graphene as a matrix for the analysis of low molecular weight compounds. In positive ion mode, besides $[M + H]^+$, the analytes were also detected in the form of multiple adduct ions such as sodium adduct $[M + Na]^+$ and double sodium adduct $[M + 2Na\text{-}H]^+$. Compared with conventional matrixes such as CHCA, graphene as matrix had several advantages including simple sample preparation, higher efficiency in desorption/ionization of analyte, and improved reproducibility of peak intensities. Lu et al. [93] employed graphene as matrix in negative mode of MS for the analysis of amino peptides, acids, and fatty acids. Their work demonstrated that only deprotonated monomeric species $[M\text{-}H]^-$ ions were homogeneously obtained on uniform graphene flakes film when negative ion mode was applied. Also, Ling et al. [94] used graphene as probe to detect ssDNA. In their work, graphene can be used as an ultrahigh efficiency preconcentration and detection platform for ssDNA. DNA-adsorbed graphene can be used directly for

SALDI-MS detection without using other matrixes and further labeling. Zhang et al. [95] reported graphene as matrix to analyze polycyclic aromatic hydrocarbons and estrogen. This method could efficiently ionize nonpolar molecules that were hardly ionized by traditional method. The π–π stacking helped the ionization process because the ionization signal increased with the increasing of benzene ring numbers in the PAHs. Li et al. [96] studied different effects of graphene-based nanomaterials, including graphene, GO, and reduced GO, in the analysis of flavonoids by SALDI-TOF MS. They concluded that GO was the most suitable matrix, and GO sheets of larger lateral size resulted in better desorption/ionization efficiency.

In analyte solutions, graphene would aggregate easily, leading to the decrease in enrich efficiency. Compared with graphene, GO has more polar moieties on its surface, so it has better solubility and dispersibility. Zhang et al. [97] employed reduced GO films as matrix for the detection of octachlorodibenzo-*p*-dioxin. In this work the problem of "sweet spot" was avoided and the detection limit was as low as 500 pg, which is the best result up to now. Liu et al. [98] used it to detect tetracyclines from the milk samples, and tetracyclines were effectively enriched with the limit of detection (LOD) as low as 2 nM in this work.

Sometimes, graphene-related materials also could enrich background molecules, which was not expected. Basri et al. [99] immobilized thiol-functionalized cocaine and adenosine aptamers onto GO by disulfide bond in order to overcome the non-specific adsorption of GO and then used this modified GO to enrich cocaine and adenosine. GO could transfer energy by conjugated p–p interactions, so the aptamer- conjugated GO played as dual roles for selective enrichment and MS matrix. Jieon et al. [100] developed a new matrix by composing GO and carbon nanotube. They immobilized this material on the substrate and realized quantitative analysis of phospholipase activity assays.

Moreover, how to separate graphene-related materials from the solution was still a tough work, and magnetization is a facial way. Deng et al. [101, 102] used the simple hydrothermal method to load Fe_3O_4 particle on graphene and nanotube. After extraction, the composite can easily be separated from the solution by external magnet. So, magnetic NP-based composed carbon materials will have high potential in this field.

Nanostructure-Initiator Mass Spectrometry (NIMS)

In modern biology study, researchers are eager to acquire the information of not only the compositions in a sample but also the spatial distribution of certain species. Traditional methods, such as magnetic resonance imaging (MRI), positron emission computed tomography (PET), and fluorescence imaging, are puzzled by low-resolution or complicated sample preparation [103–105]. To solve these problems, researchers combined MS that is a high sensitive method for the identification and determination of various molecules from small ones to large biomolecules, with imaging technique to create mass spectrometry imaging (MSI). MSI is a label-free

and high-resolution method allowing the investigation of the spatial distribution of molecules on different surfaces [106]. It can show details of biological processes on a large scale from subcellular to whole biological systems [107].

MSI is usually classified by the type of ion sources utilized in MS. The most commonly used methods are secondary ion mass spectrometry (SIMS), MALDI-MS, and desorption electrospray ionization mass spectrometry (DESI-MS). SIMS can achieve about 50 nm spatial resolution [108], but it produces too many fragments that limit its application in biology research. MALDI-MS, also a desorption/ionization method operated in high vacuum, is a powerful method that can produce intact large biomolecules using laser, but the spatial resolution of MALDI-MS is just 20 μm [107]. Moreover, DESI-MS [109], utilizing electrospray droplets for the desorbing of molecules from sample surface, spatial resolution is about 40–400 μm [107], which still has much space for improvement.

Northen et al. [110] reported a new ion source using nanostructured surface with roughly 10 nm pores. It is a tool used in spatially defined mass analysis called nanostructure-initiator MS (NIMS). NIMS utilized initiator molecules trapped in nanostructured surfaces to ionize and desorb the sample molecules adsorbed on the nanostructured surface. Both ions and laser can be used in NIMS to realize ionization process. When using laser, laser irradiation causes surface heating, resulting in the expansion of initiator and desorption of the absorbed analytes. Comparing with MALDI, NIMS can generate multiply charged ions. When using ion beam, it can also produce intact ion, and the ion-irradiated surfaces do not reveal any changes in surface nanostructure. These make NIMS quite different from the other surface desorption/ionization methods such as DIOS-MS. For NIMS, some available experiment conditions are shown below [110]:

- NIMS activity irradiation: nitrogen laser and ion sources (such as Au^1, Ga^1, Bi^1, and $Bi_3{}^1$)
- NIMS activity surface: native surfaces, silanized surfaces, and surfaces sputtered with Au/Pd
- Initiator molecules: auric acid, polysiloxanes, siloxanes, perfluorinated siloxanes, and silanes (molecular masses from 200 to 14,000 Da)

And the process of making a standard NIMS chips is shown below. More detailed information can be found in relevant paper [110]. First, etch low-resistivity (0.01–0.02 Ωcm) P-type $<100>$ (boron) silicon under 48 mA cm^{-2} for 30 min. Various initiators could be used on silanized or unsilanized surfaces. For laser irradiation, initiator solution was applied to the surface at 25 °C for 30–60 min and then using nitrogen to remove the excess initiator. For ion irradiation, apply a 14 kDa poly(3,3,3-trifluoropropylmethylsiloxanes) to a silanized and vacuum-baked surface, then bake the surface overnight at 100 °C, using nitrogen to remove the excess polymer, and brief rinse the surface with tert-butyl methyl ether. Figure 1 shows the principle picture of NIMS.

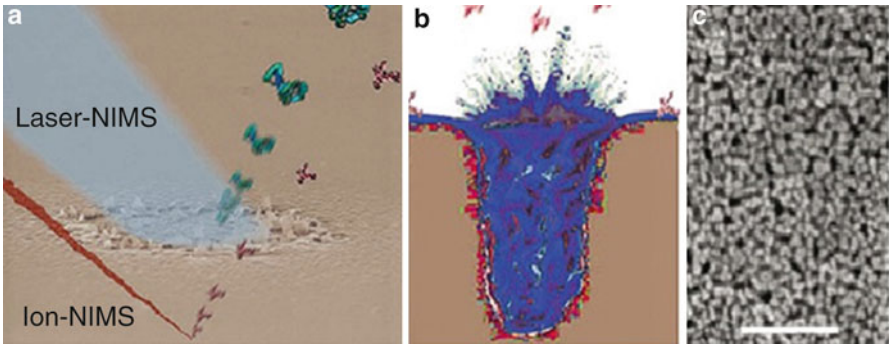

Fig. 1 (**a**) Principle picture of NIMS. The lateral resolution of ion irradiation (*red*) is much better than that of laser shot (*blue*). (**b**) Possible mechanism of the release of initiator molecules trapped in surface because of irradiation. (**c**) SEM image of 10 nm pores on the NIMS surface [110] (Adapted by permission from Macmillan Publishers Ltd.: Nature [110], copyright (2007))

Because of high lateral resolution (ion-NIMS about 150 nm), high sensitivity, matrix-free, and reduced fragmentation, NIMS is now widely used in the characterization of peptide microarrays, single cells analysis, tissue MSI, and direct analysis of blood and urine [110]. For example, Yanes et al. [111] used NIMS for tissue imaging and direct biofluid analysis using NIMS. Xenobiotics and endogenous metabolites in tissues were detected, with clozapine and *N*-desmethylclozapine observed from mouse and rat brain. Ketamine and norketamine were directly detected from plasma and urine, and the quantitative analysis was also demonstrated. Linear response and LOD of methamphetamine, codeine, alprazolam, and morphine are discussed. All of these results showed that NIMS is a powerful tool in analysis of complex biological tissues and fluids.

To sum up, NIMS is a novel and powerful spatially defined mass analysis method. With its excellent properties, it is now widely used in biology research, especially tissue imaging.

Conclusion

In this chapter, the authors discussed the applications of NPs in MS for high sensitive detection and bioanalysis. In the first part, they describe the applications of various NPs in SALDI-MS, including silicon nanomaterials, metallic nanomaterials, metal oxide nanomaterials, and carbon-based nanomaterials. In the second part, they focus on the development of NP-based new ionization source for MS. All of these examples demonstrate the great potential of NPs in the development of MS.

Under the guidance of current theory, the design and synthesis of NPs with high selectivity, stability, reusability, and efficiency are the future orientation of NPs applied in SALDI-MS. In their opinion, magnetic NP-based composed NPs will

have high potential in this field because magnetic NPs allow for fast and convenient separation from the solution by external magnet. Another reason is that composition with other functionalized NPs could enable magnetic NPs featured properties and ensure specific interactions with target analytes. Besides, the explanations for mechanism of NPs in SALDI-MS remain unclear and need to be further investigated, which could give further guidance to the design and development of unique NPs to be used in MS.

Acknowledgment This work was financially supported by the National Natural Science Foundation of China (grant No. 21027012, 21175005 and 21275012).

References

1. M. Karas, F. Hillenkamp, Anal. Chem. **60**, 2299–2301 (1988)
2. D.J. Harvey, Mass Spectrom. Rev. **18**, 349–450 (1999)
3. M.W.F. Nielen, Mass Spectrom. Rev. **18**, 309–344 (1999)
4. C. Fenselau, P.A. Demirev, Mass Spectrom. Rev. **20**, 157–171 (2001)
5. J.O. Lay, Mass Spectrom. Rev. **20**, 172–194 (2001)
6. K. Tang, D. Opalsky, K. Abel, D. van den Boom, P. Yip, G. Del Mistro, A. Braun, C.R. Cantor, Int. J. Mass Spectrom. **226**, 37–54 (2003)
7. R. Knochenmuss, Analyst **131**, 966–986 (2006)
8. R. Zenobi, R. Knochenmuss, Mass Spectrom. Rev. **17**, 337–366 (1998)
9. T.K. Sau, A.L. Rogach, Adv. Mater. **22**, 1781–1804 (2010)
10. C. Chang, X. Wang, Y. Bai, H. Liu, TrAC Trends Anal. Chem. **39**, 195–206 (2012)
11. C.K. Chiang, W.T. Chen, H.T. Chang, Chem. Soc. Rev. **40**, 1269–1281 (2011)
12. K. Tanaka, H. Waki, Y. Ido, S. Akita, Y. Yoshida, T. Yashida, Rapid Commun. Mass Spectrom. **2**, 151–153 (1988)
13. M. Schurenberg, K. Dreisewerd, F. Hillenkamp, Anal. Chem. **71**, 221–229 (1999)
14. J. Wei, J.M. Buriak, G. Siuzdak, Nature **399**, 243–246 (1999)
15. D.S. Peterson, Mass Spectrom. Rev. **26**, 19–34 (2007)
16. K.P. Law, J.R. Larkin, Anal. Bioanal. Chem. **399**, 2597–2622 (2011)
17. Z.X. Shen, J.J. Thomas, C. Averbuj, K.M. Broo, M. Engelhard, J.E. Crowell, M.G. Finn, G. Siuzdak, Anal. Chem. **73**, 612–619 (2001)
18. A. Gorecka-Drzazga, S. Bargiel, R. Walczak, J.A. Dziuban, A. Kraj, T. Dylag, J. Silberring, Sens. Actuators B Chem. **103**, 206–212 (2004)
19. S. Tuomikoski, K. Huikko, K. Grigoras, P. Ostman, R. Kostiainen, M. Baumann, J. Abian, T. Kotiaho, S. Franssila, Lab Chip **2**, 247–253 (2002)
20. J.D. Cuiffi, D.J. Hayes, S.J. Fonash, K.N. Brown, A.D. Jones, Anal. Chem. **73**, 1292–1295 (2001)
21. T. Seino, H. Sato, A. Yamamoto, A. Nemoto, M. Torimura, H. Tao, Anal. Chem. **79**, 4827–4832 (2007)
22. N.H. Finkel, B.G. Prevo, O.D. Velev, L. He, Anal. Chem. **77**, 1088–1095 (2005)
23. Y. Coffinier, S. Janel, A. Addad, R. Blossey, L. Gengembre, E. Payen, R. Boukherroub, Langmuir **23**, 1608–1611 (2007)
24. G.H. Luo, Y. Chen, H. Daniels, R. Dubrow, A. Vertes, J. Phys. Chem. B **110**, 13381–13386 (2006)
25. E.P. Go, J.V. Apon, G.H. Luo, A. Saghatelian, R.H. Daniels, V. Sahi, R. Dubrow, B.F. Cravatt, A. Vertes, G. Siuzdak, Anal. Chem. **77**, 1641–1646 (2005)
26. X. Li, P.W. Bohn, Appl. Phys. Lett. **77**, 2572–2574 (2000)
27. R.A. Kruse, X.L. Li, P.W. Bohn, J.V. Sweedler, Anal. Chem. **73**, 3639–3645 (2001)

28. Q. Li, A. Ricardo, S.A. Benner, J.D. Winefordner, D.H. Powell, Anal. Chem. **77**, 4503–4508 (2005)
29. C.W. Tsao, P. Kumar, J.K. Liu, L. Devoe, Anal. Chem. **80**, 2973–2981 (2008)
30. G. Piret, H. Drobecq, Y. Coffinier, O. Melnyk, R. Boukherroub, Langmuir **26**, 1354–1361 (2010)
31. G. Piret, Y. Coffinier, C. Roux, O. Melnyk, R. Boukherroub, Langmuir **24**, 1670–1672 (2008)
32. K.P. Law, Int. J. Mass Spectrom. **290**, 47–59 (2010)
33. H. Yan, N. Xu, W.Y. Huang, H.M. Han, S.J. Xiao, Int. J. Mass Spectrom. **281**, 1–7 (2009)
34. M. Dupre, C. Enjalbal, S. Cantel, J. Martinez, N. Megouda, T. Hadjersi, R. Boukherroub, Y. Coffinier, Anal. Chem. **84**, 10637–10644 (2012)
35. S.H. Kim, A. Lee, J.Y. Song, S.Y. Han, J. Am. Soc. Mass Spectrom. **23**, 935–941 (2012)
36. S.H. Kim, J. Kim, D.W. Moon, S.Y. Han, J. Am. Soc. Mass Spectrom. **24**, 167–170 (2013)
37. Q.C. Zhang, H.F. Zou, Z. Guo, Q. Zhang, X.M. Chen, J.Y. Ni, Rapid Commun. Mass Spectrom. **15**, 217–223 (2001)
38. M. Dupre, S. Cantel, J.O. Durand, J. Martinez, C. Enjalbal, Anal. Chim. Acta **741**, 47–57 (2012)
39. K. Agrawal, H.F. Wu, Rapid Commun. Mass Spectrom. **22**, 283–290 (2008)
40. Y.F. Sha, C.H. Deng, B.Z. Liu, J. Chromatogr. A **1198**, 27–33 (2008)
41. A.Y. Lim, F. Gu, Z. Ma, J. Ma, F. Rowell, Analyst **136**, 2775–2785 (2011)
42. P.X. Zhao, X.F. Guo, H. Wang, C.B. Qi, H.S. Xia, H.S. Zhang, Anal. Bioanal. Chem. **402**, 1041–1056 (2012)
43. Z.C. Xiong, L.Y. Zhang, R.S. Zhang, Y.R. Zhang, J.H. Chen, W.B. Zhang, J. Sep. Sci. **35**, 2430–2437 (2012)
44. J.A. McLean, K.A. Stumpo, D.H. Russell, J. Am. Chem. Soc. **127**, 5304–5305 (2005)
45. F. Gamez, P. Hurtado, P.M. Castillo, C. Caro, A.R. Hortal, P. Zaderenko, B. Martinez-Haya, Plasmonics **5**, 125–133 (2010)
46. M.C. Wahl, H.S. Kim, T.D. Wood, S.H. Guan, A.G. Marshall, Anal. Chem. **65**, 3669–3676 (1993)
47. R. Nayak, D.R. Knapp, Anal. Chem. **79**, 4950–4956 (2007)
48. B.N.Y. Vanderpuije, G. Han, V.M. Rotello, R.W. Vachet, Anal. Chem. **78**, 5491–5496 (2006)
49. J. Tang, Y.C. Liu, D.W. Qi, G.P. Yao, C.H. Deng, X.M. Zhang, Proteomics **9**, 5046–5055 (2009)
50. C.H. Teng, K.C. Ho, Y.S. Lin, Y.C. Chen, Anal. Chem. **76**, 4337–4342 (2004)
51. T.C. Chiu, L.C. Chang, C.K. Chiang, H.T. Chang, J. Am. Soc. Mass Spectrom. **19**, 1343–1346 (2008)
52. M.T. Wang, M.H. Liu, C.R.C. Wang, S.Y. Chang, J. Am. Soc. Mass Spectrom. **20**, 1925–1932 (2009)
53. H. Kawasaki, T. Yonezawa, T. Watanabe, R. Arakawa, J. Phys. Chem. C **111**, 16278–16283 (2007)
54. T. Yonezawa, H. Kawasaki, A. Tarui, T. Watanabe, R. Arakawa, T. Shimada, F. Mafune, Anal. Sci. **25**, 339–346 (2009)
55. H. Kawasaki, T. Yao, T. Suganuma, K. Okumura, Y. Iwaki, T. Yonezawa, T. Kikuchi, R. Arakawa, Chem. Eur. J. **16**, 10832–10843 (2010)
56. H. Sonderegger, C. Rameshan, H. Lorenz, F. Klauser, M. Klerks, M. Rainer, R. Bakry, C.W. Huck, G.K. Bonn, Anal. Bioanal. Chem. **401**, 1963–1974 (2011)
57. G. Piret, D. Kim, H. Drobecq, Y. Coffinier, O. Melnyk, P. Schmuki, R. Boukherroub, Analyst **137**, 3058–3063 (2012)
58. C.T. Chen, Y.C. Chen, Anal. Chem. **77**, 5912–5919 (2005)
59. K.-H. Lee, C.-K. Chiang, Z.-H. Lin, H.-T. Chang, Rapid Commun. Mass Spectrom. **21**, 2023–2030 (2007)
60. T.-C. Chiu, Talanta **86**, 415–420 (2011)
61. T. Watanabe, K. Okumura, K. Nozaki, H. Kawasaki, R. Arakawa, Rapid Commun. Mass Spectrom. **23**, 3886–3890 (2009)

62. K. Shrivas, T. Hayasaka, Y. Sugiura, M. Setou, Anal. Chem. **83**, 7283–7289 (2011)
63. T. Watanabe, H. Kawasaki, T. Yonezawa, R. Arakawa, J. Mass Spectrom. **43**, 1063–1071 (2008)
64. W.J. Shin, J.H. Shin, J.Y. Song, S.Y. Han, J. Am. Soc. Mass Spectrom. **21**, 989–992 (2010)
65. W.-Y. Chen, Y.-C. Chen, Anal. Bioanal. Chem. **386**, 699–704 (2006)
66. Y. Iwaki, H. Kawasaki, R. Arakawa, Anal. Sci. **28**, 893–900 (2012)
67. M.J. Yuan, Z. Shan, B.Z. Tian, B. Tu, P.Y. Yang, D.Y. Zhao, Microporous Mesoporous Mater. **78**, 37–41 (2005)
68. Y. Gholipour, S.L. Giudicessi, H. Nonami, R. Erra-Balsells, Anal. Chem. **82**, 5518–5526 (2010)
69. H. Kataura, Y. Kumazawa, Y. Maniwa, I. Umezu, S. Suzuki, Y. Ohtsuka, Y. Achiba, Synth. Met. **103**, 2555–2558 (1999)
70. J. Sandler, M.S.P. Shaffer, T. Prasse, W. Bauhofer, K. Schulte, A.H. Windle, Polymer **40**, 5967–5971 (1999)
71. S. Berber, Y.K. Kwon, D. Tomanek, Phys. Rev. Lett. **84**, 4613–4616 (2000)
72. M.F. Yu, B.S. Files, S. Arepalli, R.S. Ruoff, Phys. Rev. Lett. **84**, 5552–5555 (2000)
73. S.Y. Xu, Y.F. Li, H.F. Zou, J.S. Qiu, Z. Guo, B.C. Guo, Anal. Chem. **75**, 6191–6195 (2003)
74. W.Y. Chen, L.S. Wang, H.T. Chiu, Y.C. Chen, C.Y. Lee, J. Am. Soc. Mass Spectrom. **15**, 1629–1635 (2004)
75. S.F. Ren, Y.L. Guo, Rapid Commun. Mass Spectrom. **19**, 255–260 (2005)
76. C.S. Pan, S.Y. Xu, L.G. Hu, X.Y. Su, J.J. Ou, H.F. Zou, Z. Guo, Y. Zhang, B.C. Guo, J. Am. Soc. Mass Spectrom. **16**, 883–892 (2005)
77. J. Meng, C. Shi, C. Deng, Chem. Commun. **47**, 11017–11019 (2011)
78. S.-F. Ren, Y.-L. Guo, J. Am. Soc. Mass Spectrom. **17**, 1023–1027 (2006)
79. K. Shrivas, H.-F. Wu, J. Mass Spectrom. **45**, 1452–1460 (2010)
80. X.-S. Li, J.-H. Wu, L.-D. Xu, Q. Zhao, Y.-B. Luo, B.-F. Yuan, Y.-Q. Feng, Chem. Commun. **47**, 9816–9818 (2011)
81. S. Margadonna, K. Prassides, J. Solid State Chem. **168**, 639–652 (2002)
82. J.H. Schon, C. Kloc, T. Siegrist, M. Steigerwald, C. Svensson, B. Batlogg, Nature **413**, 831–833 (2001)
83. J. Havel, J. Soto-Guerrero, J. Radioanal. Nucl. Chem. **263**, 489–492 (2005)
84. G. Montsko, A. Vaczy, G. Maasz, E. Mernyak, E. Frank, C. Bay, Z. Kadar, R. Ohmacht, J. Wolfling, L. Mark, Anal. Bioanal. Chem. **395**, 869–874 (2009)
85. J.T. Shiea, J.P. Huang, C.F. Teng, J.Y. Jeng, L.Y. Wang, L.Y. Chiang, Anal. Chem. **75**, 3587–3595 (2003)
86. M.V. Ugarov, T. Egan, D.V. Khabashesku, J.A. Schultz, H.Q. Peng, V.N. Khabashesku, H. Furutani, K.S. Prather, H.W.J. Wang, S.N. Jackson, A.S. Woods, Anal. Chem. **76**, 6734–6742 (2004)
87. R.M. Vallant, Z. Szabo, L. Trojer, M. Najam-ul-Haq, M. Rainer, C.W. Huck, R. Bakry, G.K. Bonn, J. Proteome Res. **6**, 44–53 (2007)
88. D.R. Dreyer, R.S. Ruoff, C.W. Bielawski, Angew. Chem. Int. Ed. **49**, 9336–9344 (2010)
89. K.S. Novoselov, A.K. Geim, S.V. Morozov, D. Jiang, Y. Zhang, S.V. Dubonos, I.V. Grigorieva, A.A. Firsov, Science **306**, 666–669 (2004)
90. C.N.R. Rao, A.K. Sood, K.S. Subrahmanyam, A. Govindaraj, Angew. Chem. Int. Ed. **48**, 7752–7777 (2009)
91. W.S. Hummers, R.E. Offeman, J. Am. Chem. Soc. **80**, 1339 (1958)
92. X. Dong, J. Cheng, J. Li, Y. Wang, Anal. Chem. **82**, 6208–6214 (2010)
93. M. Lu, Y. Lai, G. Chen, Z. Cai, Anal. Chem. **83**, 3161–3169 (2011)
94. L.A.L. Tang, J. Wang, K.P. Loh, J. Am. Chem. Soc. **132**, 10976–10977 (2010)
95. J. Zhang, X. Dong, J. Cheng, J. Li, Y. Wang, J. Am. Soc. Mass Spectrom. **22**, 1294–1298 (2011)
96. C.-W. Liu, M.-W. Chien, C.-Y. Su, H.-Y. Chen, L.-J. Li, C.-C. Lai, Analyst **137**, 5809–5816 (2012)

97. X. Zhou, Y. Wei, Q. He, F. Boey, Q. Zhang, H. Zhang, Chem. Commun. **46**, 6974 (2010)
98. J. Liu, Y. Liu, M. Gao, X. Zhang, J. Am. Soc. Mass Spectrom. **23**, 1424–1427 (2012)
99. B. Gulbakan, E. Yasun, M.I. Shukoor, Z. Zhu, M. You, X. Tan, H. Sanchez, D.H. Powell, H. Dai, W. Tan, J. Am. Chem. Soc. **132**, 17408–17410 (2010)
100. J. Lee, Y.-K. Kim, D.-H. Min, J. Am. Chem. Soc. **132**, 14714–14717 (2010)
101. C. Shi, J. Meng, C. Deng, Chem. Commun. **48**, 2418–2420 (2012)
102. C. Shi, J. Meng, C. Deng, J. Mater. Chem. **22**, 20778–20785 (2012)
103. B.N.G. Giepmans, S.R. Adams, M.H. Ellisman, R.Y. Tsien, Science **312**, 217–224 (2006)
104. T.K. Lewellen, Phys. Med. Biol. **53**, R287–R317 (2008)
105. M.L. Zierhut, E. Ozturk-Isik, A.P. Chen, I. Park, D.B. Vigneron, S.J. Nelson, J. Magn. Reson. Imaging **30**, 473–480 (2009)
106. E.R.A. van Hove, D.F. Smith, R.M.A. Heeren, J. Chromatogr. A **1217**, 3946–3954 (2010)
107. K. Chughtai, R.M.A. Heeren, Chem. Rev. **110**, 3237–3277 (2010)
108. G. Slodzian, B. Daigne, F. Girard, F. Boust, F. Hillion, Biol. Cell **74**, 43–50 (1992)
109. Z. Takats, J.M. Wiseman, B. Gologan, R.G. Cooks, Science **306**, 471–473 (2004)
110. T.R. Northen, O. Yanes, M.T. Northen, D. Marrinucci, W. Uritboonthai, J. Apon, S.L. Golledge, A. Nordstrom, G. Siuzdak, Nature **449**, 1033–U1033 (2007)
111. O. Yanes, H.K. Woo, T.R. Northen, S.R. Oppenheimer, L. Shriver, J. Apon, M.N. Estrada, M.J. Potchoiba, R. Steenwyk, M. Manchester, G. Siuzdak, Anal. Chem. **81**, 2969–2975 (2009)